Ordered End-Member of ZSM-48 Zeolite Family

C. E. A. Kirschhock,*[,†] D. Liang,[‡] G. Van Tendeloo,[‡] A. Fécant,[§] G. Hastoye,[†] G. Vanbutsele,[†] N. Bats,[§] E. Guillon,[§] and J. A. Martens[†]

Center for Surface Chemistry and Catalysis, K. U. Leuven, Kasteelpark Arenberg 23, B-3001 Heverlee, Belgium, EMAT, University of Antwerp, Groenenborgerlaan 171, B-2020 Antwerp, Belgium, and IFP-Lyon, Rond-Point de l'échangeur de Solaize, BP 3, 69360 Solaize, France

Received September 25, 2008. Revised Manuscript Received November 24, 2008

ZSM-48 and related zeolites are considered to be highly disordered structures. Different polytypes can be clearly distinguished by simulation of high-resolution electron microscopy images. Synthesis of phase-pure polytypes was attempted. One of the investigated samples crystallized via seeding designated as COK-8 consisted of nanoscopic, needlelike crystals with a very large length/width ratio, growing along the pore direction. These specimens are phase-pure polytype 6 (PT6, numbering according to Lobo and van Koningsveld). Aggregates of these nanoneedles occasionally contained a second polytype: PT1. The latter polytype occurred more abundantly in larger crystal rods in an IZM-1 sample crystallized in ethylene glycol. Here too, the isolated crystallites mainly consist of large, defect-free regions of PT6. A simulation of polytype lattice energies offers a rational explanation for the observed polytypical intergrowth formation.

Introduction

ZSM-48 zeolite was first discovered as an impurity phase growing epitaxially from the octahedral habits of ZSM-39 crystals.[1] Later on, many synthesis recipes were reported for the synthesis of ZSM-48, ZBM-30, EU-11, and EU-2 zeolites all showing a similar X-ray diffraction pattern.[2−20] The variety of organic templates including organic linear amine and polyamine compounds, diquaternary alkyl ammonium compounds, and glycols that have been used successfully to prepare these phases reveals the synthesis of a ZSM-48 type zeolite is not very demanding with respect to the structure directing function of the organic template. The use of ZSM-48 seeds triggers the crystallization of ZSM-48 type zeolite even from a synthesis mixture with a nonspecific template such as tetramethylammonium cation (TMA),[21] whereas heterostructural seeding promotes the crystallization of ZSM-48 phases in the presence of appropriate long linear organic molecules fitting with the pores.[20]

Schlenker et al. were the first to propose a ZSM-48 structure model based on ferrierite sheets.[22] Different configurations of four independent T-atoms (tetrahedrally coordinated framework atoms) of these sheets resulted in 28 closely related structures with different symmetries, among which two were found to show good agreement between simulated and experimental XRD patterns: UUDD-*Cmcm* and UDUD-*Imma*. An intergrowth of these two polytypes (PTs) was proposed as model of the real disordered structure. Electron microscopy was used for ZSM-48 investigation by Kirkland et al.[12] Extensive twinning perpendicular to the pore direction was observed. However, image simulation could not distinguish the two structure models proposed by Schlenker et al.,[22] as both produced similar contrasts for the applied experimental conditions at that time.

A more recent description of the disorder was developed by Lobo and van Koningsveld.[23] That model describes ZSM-48 as a family of disordered materials assembled from silicate tubes, entirely made up from 6-rings similar to (5,0) carbon nanotubes. As for most silicates, Si can be partially replaced by other elements with preference for tetrahedral coordination by oxygen such as aluminum. The parallel, straight channels of ZSM-48 are made up from 10 T-atoms and are linked to four neighboring tubes. Connection occurs either via 4-rings (4R) using a mirror operation or via crankshaft chains (CS) using a glide-mirror operation with reference to the con-

* Corresponding author. E-mail: Christine.kirschhock@biw.kuleuven.be.
† K. U. Leuven.
‡ University of Antwerp.
§ IFP-Lyon.

(1) Schlenker, J. L.; Dwyer, F. G.; Jenkins, E. E.; Rohrbaugh, W. J.; Kokotailo, G. T. *Nature* **1981**, *294*, 340.
(2) Rollmann, L. D.; Valyocsik, E. W. EP 0015132, 1980.
(3) Chu, P. EP 0023089, 1980.
(4) Marosi, L.; Schwarzmann M.; Stabenow, J. EP 0046504, 1981.
(5) Chu, P. USP 4397827, 1983.
(6) Rollmann, L. D.; Valyocsik, E. W. USP 4423021, 1983.
(7) Chu, P. USP 4448675, 1984.
(8) Araya, A.; Lowe, B. M. *J. Catal.* **1984**, *85*, 135.
(9) Valyocsik, E. W. EP 0142317, 1984.
(10) Valyocsik, E. W. USP 4 585 747, 1986.
(11) Jacobs, P. A.; Martens, J. A. *Stud. Surf. Sci. Catal.* **1987**, *33*, 275.
(12) Kirkland, A. I.; Millward, G. R.; Carr, S. W.; Edwards, P. P.; Klinowski, J. *ACS Symp. Ser.* **1989**, *398*, 574.
(13) Degnan, T. F.; Valyocsik, E. W. USP 5 075 269, 1991.
(14) Giordano, G.; Dewaele, N.; Gabelica, Z.; Nagy, J. B.; Derouane, E. G. *Appl. Catal.* **1991**, *71*, 79.
(15) Casci, J. L.; Lowe, B. M.; Whittam, T. V. USP 5098685, 1992.
(16) Calabro, D. C. USP 5194410, 1993.
(17) Kennedy, C. L.; Rollmann, L. D.; Schlenker, J. L. USP 5961951, 1999.
(18) Elomani; S. USP 0085976, 2002.
(19) Mériaudeau, P.; Vu Tuan, A.; Lefebcre, F.; Nghiem, V. T.; Naccache, C. *J. Catal.* **1999**, *185*, 435.
(20) Lai, W. F.; Saunders, R. B.; Mertens, M. M.; Verduijn, J. P. USP 6923949, 2005.
(21) Suzuki, K.; Hayakawa, T. *Microporous Mesoporous Mater.* **2005**, *77*, 131.
(22) Schlenker, J. L.; Rohrbaugh, W. J.; Chu, P.; Valyocsik, E. W.; Kokotailo, G. T. *Zeolites* **1985**, *5* (6), 355.
(23) Lobo, R. F.; van Koningsveld, H. *J. Am. Chem. Soc.* **2002**, *124*, 13222.

10.1021/cm802614x CCC: $40.75
Published on Web 12/30/2008

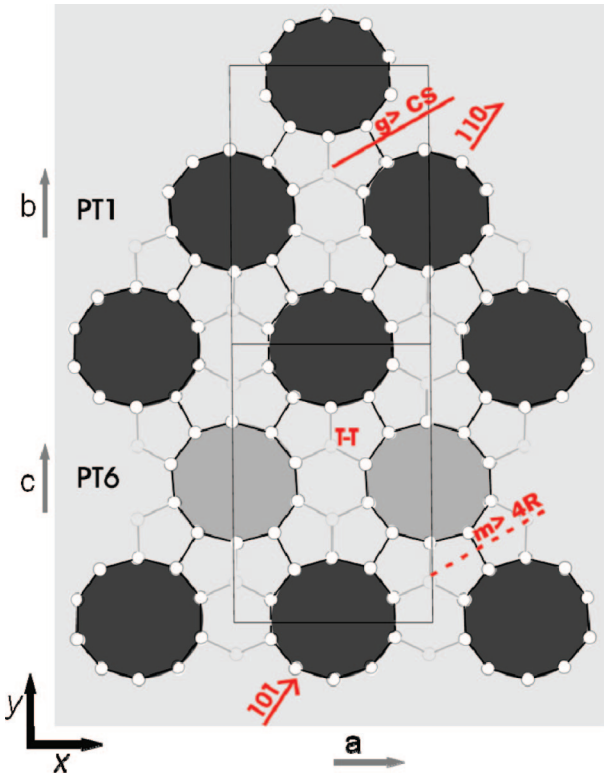

Figure 1. Illustration of the structures of PT1 (top) and PT6. Dark grey tubes are shifted by 1/2 along the *z*-axis (channel direction) in the drawing, for clarity only the positions of T atoms are shown. In PT1, linked channels are related by glidemirror planes (g) resulting in connection via crankshaft chains (CS). In PT6, channels are connected via 4-rings (4R) and the channels are related by mirror planes (m). In the center of 4-channel rhombs, T dimers (T−T) complete the crystallographic network.

necting silica-tubes (Figure 1). Four connected pores form a rhomb with an angle close to the tetrahedral angle of 109.5°. In the center of the rhombs, additional T atoms indirectly link opposite channels. In the crystallographic description these T atoms form dimers (T−T) along the channel direction. The occupancy of these T atom positions was thought to be partial and more or less disordered in real samples.[23] The symmetry of the pores allows for transformation of 4R to CS connectivity by translation of one tube by 1/2 of the lattice constant in the channel direction (Figure 2). This scheme gives rise to a series of simplest ordered polytypes, with PT1 and PT6 equivalent to the two structure models proposed earlier by Schlenker et al.[22] The model by Lobo and van Koningsveld describes the PTs as stacking of sheets of directly connected tubes. In the orthorhombic settings of PT1 and PT6 these sheets lie in the 101 and 110 planes, respectively. In PT1, all channels in layers have the same relative shift along the channel direction (dark grey in Figure 1). In PT6, neighboring tubes alternate in shift by 1/2 of the channel direction (light grey in Figure 1). Even though all PTs and disordered materials have identical channels, the structure of the crystal surface with the channel openings is defined by the relative stacking of the silica tubes (Figure 2). Especially this feature decides the selectivity of any pore-mouth or key-lock catalysis occurring in hydrocarbon processing.[24,25]

X-ray diffraction patterns of ZSM-48 and related zeolites usually show broadened reflections, which customarily is attributed to systematic stacking disorder, which has been directly observed in samples consisting of medium to large crystals.[12] Besides this type of broadening, the often observed needlelike habits of the crystallites can significantly contribute to confusion of the diffraction signals by anisotropic size broadening and preferred orientation effects. To make a distinction between the different causes for line broadening even more difficult, the degree of disorder in ZSM-48 strongly depends on the morphology of the samples.[23] Therefore, a clear analysis of nanocrystalline ZSM-48 samples by X-ray powder diffraction is greatly encumbered. A further hindrance is based on the structural similarities of the different stacking possibilities. Powder diffraction patterns of different PTs greatly resemble each other and breaking a symmetry element in one structure, for instance, because of the presence of disordered extra-framework ions or molecules, results in the occurrence of reflections usually associated with lower symmetry members of the same disorder family. Mainly as a direct result of the recurring unspecific X-ray pattern, the name "ZSM-48" has been used for a range of materials synthesized differently and probably having different degrees of disorder.[23] Other materials belonging to this disordered zeolite family have been given specific names such as ZBM-30, EU-2, and EU-11.[4,8,15]

Transmission electron microscopy (TEM) has been demonstrated to be highly useful for analysis of zeolite frameworks and local structure investigation.[26−28] In the present work, electron diffraction and high-resolution electron microscopy were employed to revisit ZSM-48 like structures. Two very different syntheses were applied to obtain samples of different morphology. The first synthesis, involving seeding, resulted in the formation of nanosized needles, often bunched together, whereas the second synthesis, in organic medium, resulted in large crystalline rods. The phases present in these two samples and the degree of intergrowth formation could be fully determined using TEM analysis. It has been possible to reveal the existence of a pure PT6 phase. A calculation of the lattice energy and elastic constants of the different PT frameworks was performed in an attempt to find an explanation for the experimental observation of PT6 as the most stable polytype.

Experimental Section

Synthesis of COK-8. The seeds for the synthesis of COK-8 were crystallized as follows: 7.75 g of KOH was dissolved in 27 g of deionized water. To this solution was added 16.7 g of 1,6-diaminohexane (Acros) dissolved in 150 g of water. Subsequently,

(24) Martens, J. A.; Souverijns, W.; Verrelst, W. H.; Parton, R. F.; Froment, G. F.; Jacobs, P. A. *Angew. Chem., Int. Ed.* **1995**, *34*, 2528.
(25) Martens, J. A.; Vanbutsele, G.; Jacobs, P. A.; Denayer, J. F.; Ocakoglu, R.; Baron, G. V.; Muñoz Arroyo, J. A.; Thybaut, J.; Marin, G. B. *Catal. Today* **2001**, *65*, 111.
(26) Anderson, M. W.; Ohsuna, T.; Sakamoto, Y.; Liu, Z.; Carlsson, A.; Terasaki, O. *Chem. Commun.* **2004**, 907.
(27) Kirschhock, C. E. A.; Bons, A.-J.; Mertens, M.; Ravishankar, R.; Mortier, W.; Martens, J. A. *Chem. Mater.* **2005**, *17*, 5618.
(28) Corma, A.; Moliner, M.; Cantin, A.; Diaz-Cabanas, M. J.; Jorda, J. L.; Zhang, D.; Sun, J.; Jansson, K.; Hovmöller, S.; Zou, X. *Chem. Mater.* **2008**, *20*, 3218.

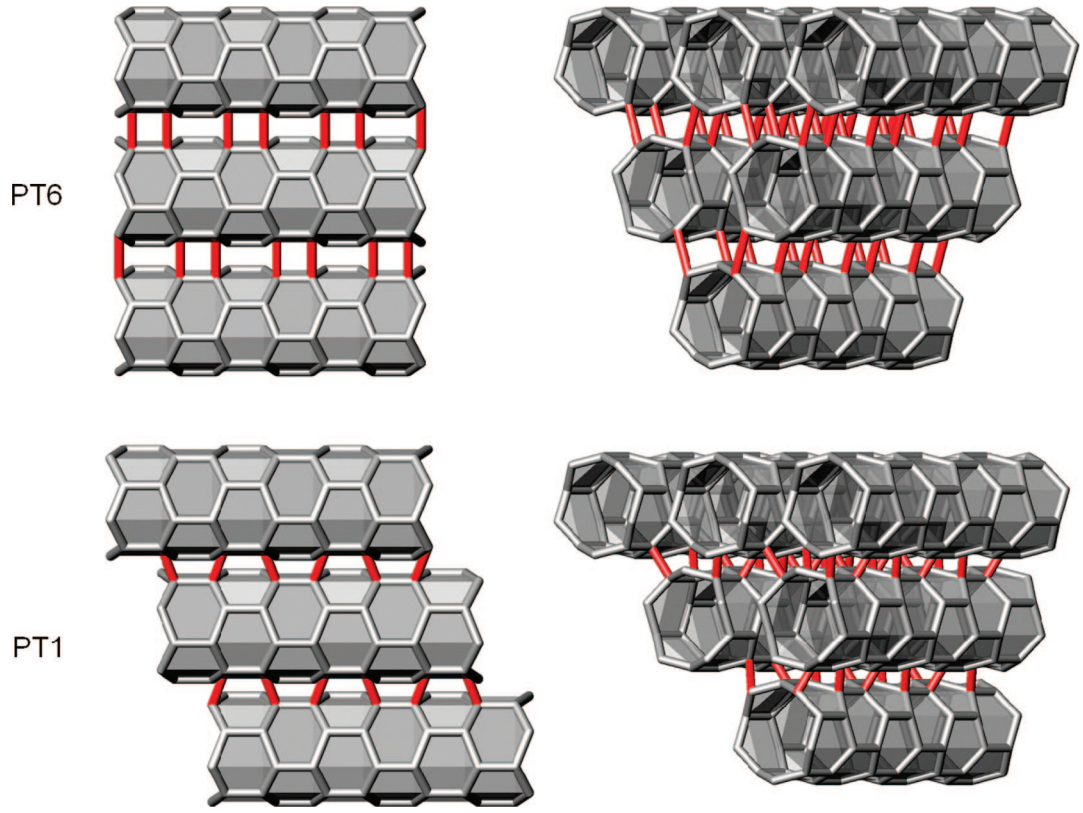

Figure 2. Illustration of channel connectivity via 4R in PT6 (top) and via CS in PT1 (bottom). For clarity, only the positions of T atoms are shown.

the obtained solution was slowly added to 72 g of Ludox AS-40 (Aldrich) diluted with 124 g of water under continuous mixing. The gel was divided equally over 4 autoclaves with a volume of 120 mL. The autoclaves were heated at 150 °C for 65 h. Agitation was achieved by tumbling of the autoclaves at ca. 60 rpm. The solid product was recovered by filtration on a Buchner funnel and washed with deionized water on the filter. The sample was dried at 60 °C in air and subsequently calcined in a tubular furnace under flow. First, the powder was heated to 400 °C under a N_2 flow and kept there for 5 h. The temperature was then raised to 550 °C under an O_2 flow and the calcination was performed overnight.

For the synthesis of COK-8 sample, 46.155 g of triethylenetetramine, 60%, Acros) was dissolved in 46.155 g of water; 7.69 g of Aerosil 380 was added, and 0.33 g of $Al(OH)_3$ (Merck). Finally, 0.66 g of seeds was added. The resulting gel was loaded into a stainless steel autoclave and heated for 88 h at 170 °C and continuously tumbled. The zeolite was recovered and calcined as done with the seeds.

Synthesis of IZM-1. IZM-1 synthesis was carried out in 160 mL stainless steel autoclaves with Rochton type stirring system. Ludox HS40 (40% SiO_2, Aldrich) was used as the silica source for the reactions. Sodium hydroxyde (>98%, Carlo Erba) was used as the source of hydroxide ions. A solution was prepared from 12.37 g of deionized water (18 MΩ), 64.52 g of ethylene glycol, and 12.37 g of 6-(dibutylamino)-1,8-diazabicyclo[5.4.0]undec-7-ene (purities of, respectively, >99% and 98%, Aldrich). Sodium hydroxide (0.83 g) was added to the solution and the mixture was stirred until dissolution of the solids. An amount of 9.97 g of Ludox HS40 was added last under stirring for 10 min. The final mixture was transferred into the stainless steel reactor and heated at 170 °C while being rotated at ca. 250 rpm for 6 days. At the end of the reaction, the solid was filtered and washed with deionized water (until pH about 7), dried one night at 120 °C, and finally calcined at 550 °C for 8 h.

Table 1. Polytype Space Groups and Lattice Constants Calculated by GULP[32−35]

	space group	*a* (Å)	*b* (Å)	*c* (Å)	*β* (deg)
PT1	*Cmcm*	14.62	20.56	8.71	
PT2	*Pmm*2	8.33	23.47	12.34	
PT3	*C*2/*m*	25.35	8.60	12.55	109.19
PT4	*Pmm*2	8.43	23.43	12.34	
PT5	*Cmcm*	8.38	24.46	23.66	
PT6	*Imma*[a]	14.64	8.49	20.52	
PT7	*Pmmn*	23.64	8.32	24.48	

[a] The unusual setting of space group 74 has been chosen to better compare with PT1.

Simulation of Lattice Coordinates of Polytypes. On the basis of the connectivity described by Lobo et al.[23] and reported in the database of disordered frameworks of the International Zeolite Association[29] the coordinates of the different polytypes were obtained with the program DLS76,[30,31] followed by relax-fitting with the GULP software,[32−34] using the Catlow library.[35] Spacegroups and lattice constants for polytypes 1 to 7 are listed in Table 1. The unusual setting of the spacegroup 74 Immb in place of *Imma* for the polytype 6 has been chosen to better compare with the structure of PT1 described in spacegroup Cmcm. GULP also served to calculate the lattice energies and mechanic properties of the PTs.

(29) Gies H. andvan Koningsveld, H. *Catalog of Disorder in Zeolite Frameworks*; available from http://www.iza-structure.org/databases/.
(30) Ch. Baerlocher, Ch., Hepp, A.; Meier, W. M. *DLS-76: A Program for the Simulation of Crystal Structures by Geometric Refinement*; Institute of Crystallography and Petrography, ETH Zurich: Zurich, Switzerland, 1977.
(31) Baerlocher, Ch.; Hepp, A. *Z. Kristallogr.* **1976**, *144*, 415.
(32) Gale, J. D.; Rohl, A. L. *Mol. Simul.* **2003**, *29*, 291.
(33) Gale, J. D. *Z. Kristallogr.* **2005**, *220*, 552.
(34) Gale, J. D.; Henson, N.J. *J. Chem. Soc., Faraday Trans.* **1994**, *90*, 3175.
(35) Catlow, C. R. A.; French, S. A.; Sokol, A. A.; Thomas, J. M. *Philos. Trans. R. Soc. London, A* **2005**, *363*, 913.

Lattice energies were compared to the lattice energy of quartz, which was calculated correspondingly.[36,37]

X-ray Diffraction. X-ray diffraction was performed in transmission geometry with $CuK_{\alpha 1}$ radiation, focusing monochromator, and 5° 2θ position sensitive detector in a range between 5 and 50° 2θ. Diffraction patterns were analyzed by Rietveld refinement using the GSAS software package.[38,39] The used spacegroups, atomic coordinates and starting lattice constants were derived as described above (Table 1). During refinement, atomic coordinates were not varied. To simulate a break of symmetry in channel direction possibly occurring in the seeds samples, we refined PT6 in space group *P*1 for this sample.

Electron Microscopy. Samples for electron microscopy were prepared by letting a few drops of mortared sample suspended in ethanol dry on a copper grid covered with a thin layer of holey carbon film. TEM experiments were carried out on Philips CM20 and Jeol 4000EX microscopes. Because of the vulnerability of zeolite samples to irradiation, working close to the resolution limit of the microscope was impossible. Therefore, a large spot size (i.e., low beam intensity) was used to reduce the electron intensity when taking high-resolution images. Fourier-filtering was applied to the experimental images to reduce noise. Simulations of electron diffraction patterns and high resolution images were done with the *MacTempas* software. To study the effect of disorder on the TEM patterns, we also used the DIFFax program to simulate a number of electron diffraction patterns.[40] Input files were generated on the basis of the coordinates derived as described above.

Results and Discussion

COK-8. The synthesis of COK-8 was inspired by the observation in the literature that seeding significantly facilitated the crystallization of ZSM-48 like zeolite, even in the absence of a specific organic template.[21] We used a relatively large number of seeds to synthesize this material in the presence of triethylenetetramine based on a recipe for synthesizing ZBM-30.[4] A low-magnification TEM image of COK-8 (Figure 3, top) shows the sample to consist of needlelike crystals (width, 15−80 nm; length, 0.5−4 μm), often aggregated with similarly oriented needles. Only occasionally individual crystallites are observed. In general, the nanoneedles tend to aggregate into bunches of different sizes, similar to what has been observed for ZSM-22 zeolite.[41]

The obtained X-ray powder pattern of COK-8 is a typical pattern encountered with ZSM-48 and related zeolites. The reflections appear to be rather unspecific and considerably broadened. The pattern can be fitted satisfactorily with the Pt6 structure, assuming size broadening perpendicular to the channel direction (Figure 3). However, because of the low resolution, no conclusion about the phase purity or occurrence of systematic faulting in the material can be drawn from the powder X-ray diffraction (PXRD). A similar sample also was studied with PXRD by Lobo and van Koningsveld,[23] who arrived at similar conclusions.

A tilt series of diffraction patterns from a typical aggregate of COK-8 nanoneedles is shown in Figure 4 (top). The otherwise sharp reflections are somewhat smeared perpendicular to the long axis of the crystals. This could be related to the presence of a few planar defects within the individual crystallites, but in this case, it most probably stems from the small width of the crystallites. A DIFFax[40] simulation of pure PT6 with a thickness corresponding to the analyzed small aggregate (20 layers) reproduced the observed streaking satisfactorily. (Figure 4, bottom) From the series of diffraction patterns and known tilting angles, the reciprocal lattice was constructed, by choosing as reciprocal unit cell the smallest periodic unit accounting for possible extinctions. In real space, this corresponds to: $a = 14.5$Å, $b = 8.5$ Å, $c = 20.1$ Å, $\alpha = \beta = \gamma = 90°$ (axis directions are arbitrarily chosen). Comparison with the theoretical lattice parameters of PTs (Table 1), reveals that only PT1 & PT6, which are equivalent to the two structure models originally proposed by Schlenker et al.,[22] show similar values.

With the indexing of the basic cell and identification of the present phase, the growth direction of the needles was determined. Figure 5 shows a picture with double exposure of both image and diffraction pattern of a typical aggregate. By indexing the diffraction pattern with the PT6 structure, it is shown that the long direction is along [010], the pore direction, as expected. Unfortunately, this sample morphology prevents observation of the structure in this direction, as the needles tend to lie flat on the grid because of their very large length/width ratio. However, sufficient differences between the PTs can be discerned from the accessible crystal orientations. Figure 6 shows simulations of a few low index axis diffraction patterns of PT1&PT6. The two PTs can be easily distinguished by diffraction patterns from PT6[100]/PT1[100] or PT6[101]/PT1[110]. The observed extinction rules in COK-8 are consistent with the cell centering encountered in PT6.

Comparing the experimental diffraction series (Figure 4) of an average size needle bunch with the simulated patterns, it can be seen that the experimental patterns all match simulations of the PT6 structure. However, some very weak spots in the PT6[101] diffraction pattern are present, which should be extinct according to *Immb* symmetry. The discrepancy can originate either from the presence of a very low amount of a second crystalline phase or from local planar defects breaking the PT6 structure symmetry. To distinguish which of the two possibilities applies, DIFFax[40] simulations of 5% PT1 or PT3 intergrown with otherwise pure PT6 was performed. This simulation revealed that isolated planar defects result in streaks instead of the observed sharp rows of reflections. On the other hand, already 2% of PT1 next to PT6 suffices to yield the rows of weak diffuse reflections with uneven l and $h = -k$, as observed in Figure 4, whereas the presence of PT3 results in an apparent doubling along the [101] direction. This and the failure to identify the

(36) Foster, M. D.; Friedrichs, O. D.; Bell, R. G.; Paz, F. A. A.; Klinowski, J. *Angew. Chem., Int. Ed.* **2003**, *42*, 3896.
(37) Foster, M. D.; Friedrichs, O. D.; Bell, R. G.; Paz, F. A. A.; Klinowski, J. *J. Am. Chem. Soc.* **2004**, *126*, 976.
(38) Larson A. C. and Von Dreele, R. B. *General Structure Analysis System (GSAS)*; Los Alamos National Laboratory Report LAUR 86−748; Los Alamos National Laboratory: Los Alamos, NM, 2000.
(39) Toby, B. H. *J. Appl. Cryst.* **2001**, *34*, 210–213.
(40) Treacy, M. M. J.; Newsam, J. M.; Deem, M. W. *Proc. R. Soc. London, A* **1991**, *433*, 499.
(41) Hayasaka, K.; Liang, D.; Huybrechts, W.; De Waele, B. R.; Houthoofd, K. J.; Eloy, P.; Gaigneaux, E. M.; Van Tendeloo, G.; Thybaut, J. W.; Marin, G. B.; Denayer, J. F. M.; Baron, G. V.; Jacobs, P. A.; Kirschhock, C. E. A.; Martens, J. A. *Chem.−Eur. J.* **2007**, *13*, 10070.

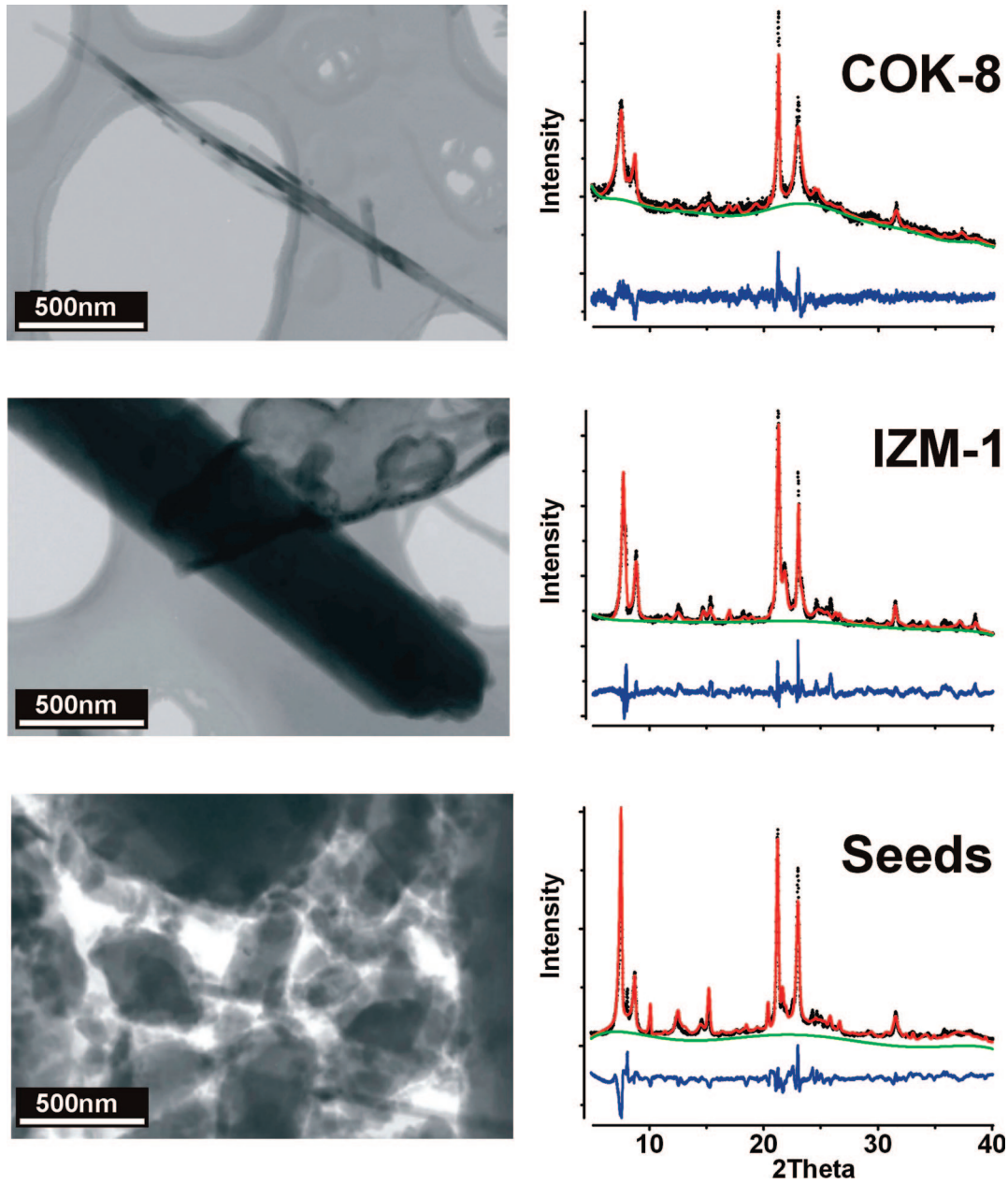

Figure 3. Low-magnification TEM and powder patterns of the samples discussed in the manuscript. From top to bottom: COK-8, IZM-1, and seeds used for COK-8 synthesis. The sharp reflection in the seed pattern at low angles is due to small amounts of TON zeolite, which was identified as a side phase by TEM (not shown).

presence of PT1 from the [100] diffraction pattern in the same tilt series, leads to the conclusion of very local occurrence of PT1 regions in the otherwise phase-pure PT6 aggregates. Figure 7 compares diffraction PT6[101] patterns of an aggregate consisting of very few needles, similar as in Figures 3 and 4, with a larger bunch of crystallites. Although the small aggregate shows a diffraction pattern of pure PT6 (Figure 7a), the larger aggregate shows the presence of PT1 more clearly (Figure 7b). The forbidden weak spots are more pronounced here and the intensity of spots $(0k0)$ and $(5k5)/(\bar{5}k5)$with $k =$ odd are lower than that of the adjacent reflections. This is a typical fingerprint of the *Cmcm* space group of PT1, as was seen from electron diffraction patterns simulated for different PTs. Only PT1 generates correct spot positions and extinctions of the $(0k0)$ spots with $k =$ odd. Generally, for aggregates thicker than 40−50 nm, reflections consistent with the extinction rules of PT1 are observed next to the very intense PT6 reflections. In the pattern of Figure 7b the additional occurrence of streaking indicates the PT1 regions either to be faulted, strained, or disordered. From these observations, we conclude that although isolated needles or their small aggregates consist almost exclusively of PT6, in larger needle bunches, PT1 is also present.

To characterize the crystallites in more detail, high-resolution electron diffraction was attempted. The simulation of high-resolution electron microscopy images for PT1 & PT6 from two orientations (see the Supporting Information) shows that clear differences can be observed for most thickness and defocus values. This result demonstrates PT6 can easily be distinguished from PT1, even at the experi-

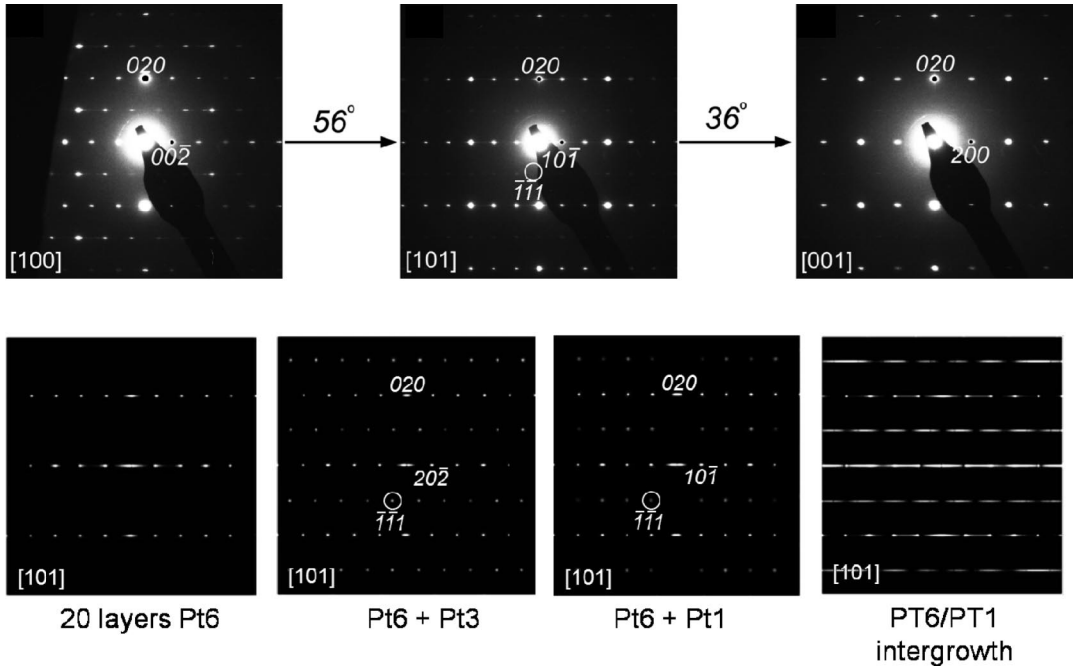

Figure 4. (Top) Electron diffraction tilt series from a nanoneedle specimen, similar to the one shown in Figure 3. The tilt angles between the diffraction patterns are indicated. Indexing according to PT6 structure. Bottom, DIFFax simulations along [101]. From left to right: (1) The slight broadening of main reflections in the experimental pattern is well described by thin stacks of PT6 layers. (2) and (3) Occurrence of the forbidden reflection in the experiment can be simulated with small amounts of PT1 next to PT6. PT3 would require a doubling of lattice constants *a* and *c*, as in this case the $(\bar{1}\bar{1}1)$ reflection would appear between spots in the $(h0\bar{l})$ direction. (4) Even low degrees of intergrowth of Pt1 in PT6 would result in extensive streaking.

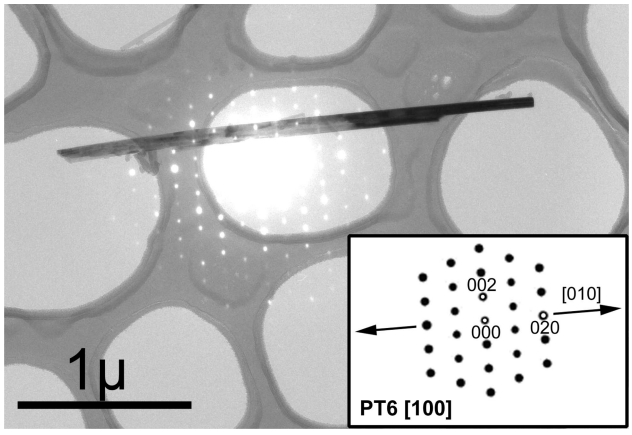

Figure 5. Double exposure to diffraction pattern and image of a small COK-8 aggregate. The long axis of the nanoneedles coincides with the channel direction of PT6.

mental resolution of about 3Å. The high resolution study reveals large defect-free areas, fully consistent with PT6. Figure 8a shows an image of the PT6[100] direction which occasionally is observed in the sample, the inset is a simulation for a defocus of 250 nm and a thickness of 90 nm; Figure 8b is an image observed close to the PT6[101] axis, the most prominently observed orientation. Two crystallites with some overlap in the middle are shown. The simulated images show excellent agreement with the experimental contrast in non-overlap areas and demonstrate the perfect alignment of the {101} faces of the nanoneedles. The inserted parts correspond to a −320 nm defocus, 30 nm thickness (left) and −350 nm defocus, 40 nm thickness (right); they were tilted away from the zone axis orientation in order to take into account the deviation from 90° of the angle between intersecting {101} faces.

Curiously enough, we never succeeded to capture PT1 or faulted regions on high-resolution images in COK-8, even when studying larger aggregates with typical reflections of the corresponding space group. This hints at PT1 being hidden within bunches of needles rather than being present in the outer thinner regions accessible to high-resolution imaging.

Summarizing the above electron diffraction results, it is reasonable to deduce that the structure of individual nanoneedles is consistent with the PT6 structure, eventually containing some local planar faults. The planar defects and the amount of PT1 increase with increasing size of the bunches of sideways aggregated nanoneedles. The needles are oriented along the [010] channel direction and are very often limited by {101} faces. These faces are simply layers of directly connected pores (Figures 1 and 2). This conclusion is also in agreement with the observations reported by Lobo and van Koningsveld on a sample, resembling in morphology our COK-8. Similar as in our case, the PXRD pattern of that sample was reported to be very similar to simulated diffraction patterns of pure PT6.[23] Most importantly, the presented ED study and HRTEM work clearly indicates a relation between local sample morphology and the occurrence of PT1 impurities.

Characterization of Seeds Used to Synthesize COK-8. COK-8 consisting of PT6 nanoneedles was synthesized using a rather large amount of seeds, synthesized in the presence of large quantities of K^+ ions. Characterization of the seeds' structure was thought to shed further light on the structural peculiarities of COK-8, especially the occurrence of PT1 exclusively within larger needle-bunches. A scanning electron microscopy (SEM) image of the seeds shows large chunks of crystalline material asides loose globular structures

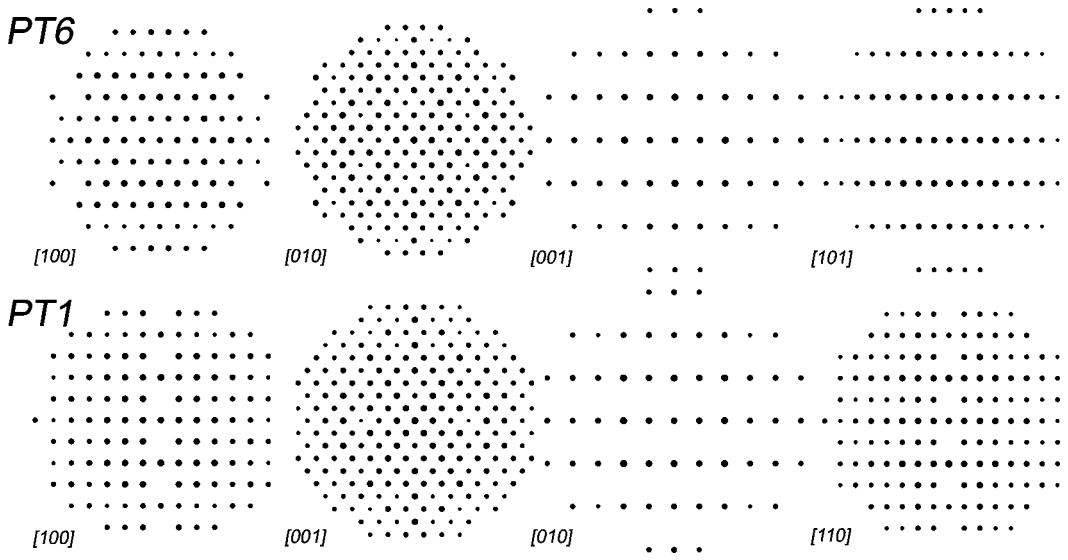

Figure 6. Simulated low index diffraction patterns from PT6 & PT1 based on spacegroups and lattice constants listed in Table 1. Comparison with Figure 4 shows that the experimental patterns all match simulations of the PT6 structure but that they also contain some weak reflections forbidden by the spacegroup of polytype 6.

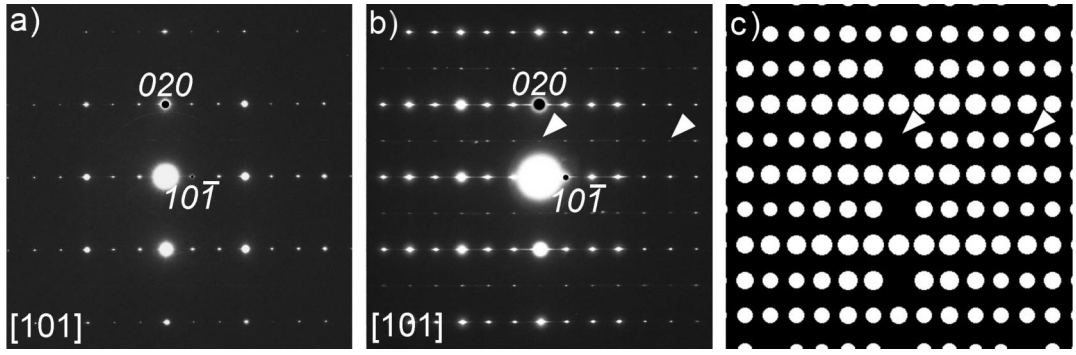

Figure 7. From left to right: Diffraction along [101] of an isolated nanoneedle, a larger bunch of nanoneedles, simulation of diffraction pattern of PT1 in the corresponding direction. The arrows indicate the systematic weakness of reflections ($5k\bar{5}$) and ($0k0$) with k uneven, typical for PT1.

(Figure 3). The PT6 material obtained from these seeds no longer contained any particles resembling the large crystals or the globular material. Therefore, it can be assumed that the seeds are fully or partially dissolved during the synthesis of the PT6 needles of the COK-8 sample.

The XRD pattern corresponding to the seeds is a typical ZSM-48 like pattern but also contains a small amount of highly crystalline TON type zeolite (Figure 3). The diffraction pattern shows reasonable crystallinity and, for this class of materials, rather sharp reflections. The intense, sharp reflections in the ED closely resemble the PT6 pattern in the [101] orientation (Figure 9). But diffuse reflections between the rows of sharp reflections indicate that either the cell centering of PT6 is not strictly followed or the occurrence of a second PT without centering. The first possibility might be due to the presence of disordered K^+ cations along the channel direction of PT6 and a probably related partial absence of the T atom dimers between four pores (Figure 9). The second possibility can be due to the presence of PT3 next to PT6 (Figure 4). The typical reflections of PT1, however, are absent so there are certainly no extended regions of this structure present. To clarify whether the sample contains both PT6 and PT3 or is better described by a disordered PT6 phase, attempts were made to fit the XRD data. A reasonable fit of the XRD pattern using PT6 and PT3 in a ratio of about 10:1 could be achieved. Still, a similar good fit was obtained using a phase pure PT6 framework with disordered K^+ ions superimposed along the channel direction (Figure 3). Considering the similar building schemes of the different PTs it comes as no surprise that breaking the symmetry of the PT6 space group generates reflections at positions usually attributed to lower symmetry PTs, like PT3. A final conclusion about the structure of this sample remains open without accurate tilting series or high-resolution TEM images. Because of the sample morphology no suitable crystallite was found for a deeper analysis of the structural details in the seeds. However, the rather sharp reflections in ED and XRD point towards extended regions of PT6 and possibly some PT3 polytype, rather than towards statistical intergrowth. The absence of PT1 in the seeds used for synthesis of COK-8 clearly indicates this PT only appears later, during growth and/or aggregation of the nanoneedles that consist of PT6.

Characterization of IZM-1. A different synthesis approach resulted in large crystalline rods with a highly resolved powder pattern (Figure 3). Rietveld analysis of this pattern revealed the presence of PT1 next to PT6 in a ratio of about 1:3. The throughout sharp reflections indicate

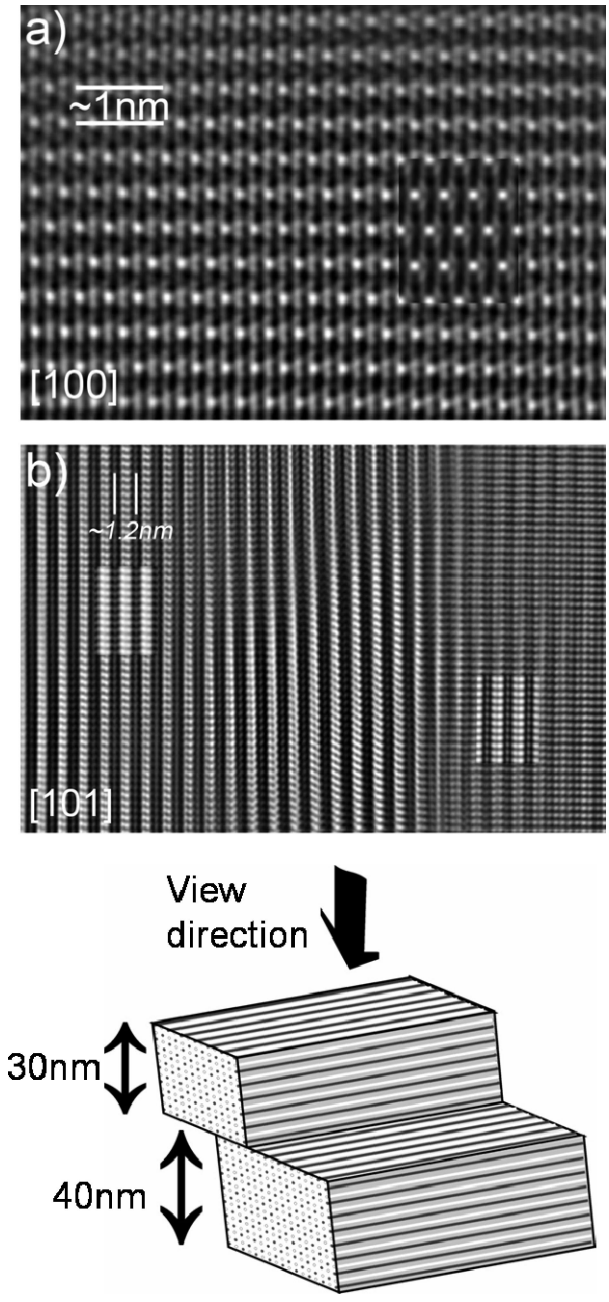

Figure 8. High-resolution images of COK-8. Large defect-free regions of PT6 are commonly encountered. Simulated patterns are superimposed on the experimental images. (a) Occasionally observed PT6[100] orientation. (b) Two overlapping crystals close to the typical [101] orientation. The simulation allowed reconstruction of the diffracting specimen (bottom). Channels are represented as lines, dark and light gray indicate relative shifts of the channels by 1/2 along *b* (crf. Figure 1).

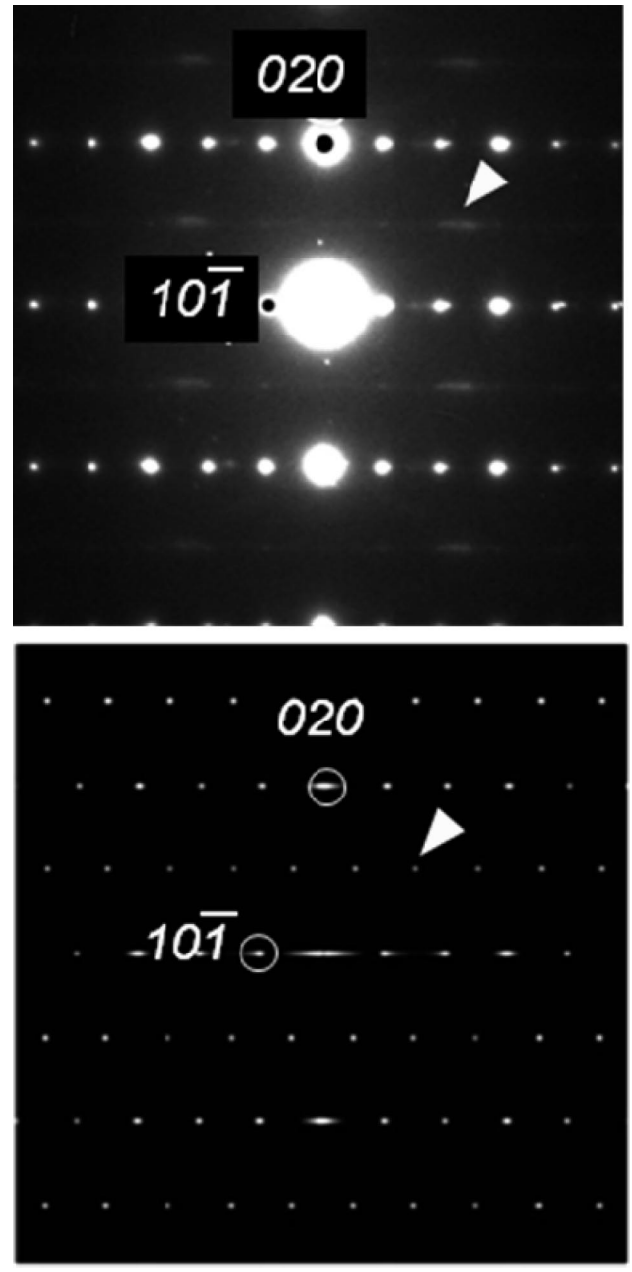

Figure 9. Experimental diffraction pattern of the seeds along [101] of PT6 (top). Rows with uneven *k* indicate the symmetry is broken along the channel axis either by presence of PT3 (crf. Figure 4) or disordered ions or molecules in the channels. A DIFFax simulation of PT6 with disordered K^+ ions is shown on the bottom. Reflections (0 2 0) and (1 0 $\bar{1}$) are marked for clarity. The occurrence of intensity indicated by an arrow which corresponds to a doubling along (h 0 $\bar{h}$) direction is due to a breaking in symmetry alond the channel direction which either can be due to presence of PT3 (crf. Figure 4) or as shown here by the presence of disordered guests.

extended regions of these two structures next to each other, rather than a disordered intergrowth. The same conclusion was drawn from a [101] ED diffraction pattern of a rod aggregate of the PT6. Very sharp reflections for both PTs are observed in this sample. Some diffuse intensity corresponding to an apparent doubling perpendicular to the [101] direction of PT6 can be taken as indication of disorder along the channel direction that can be caused by missing T atoms or might even result from disorder of the organic template present in this sample in extensive amounts. Indeed, calcined samples of the same material show much less evidence for this disorder.

TEM analysis and high-resolution imaging of individual rods revealed extended regions of PT6 with occasional planar faulting as shown in Figure 10. From the image, it is clear that a shift of 1/2 of the lattice constant in the channel direction occurs over several layers, instead of over a single layer as would be achieved by a direct interface between PT6 and PT1, as shown in Figure 1. This suggests the observed fault is rather a result of internal strain within the large crystal rather than a clear stacking fault intergrowth. The internal strain in the thin edges of the crystal could have

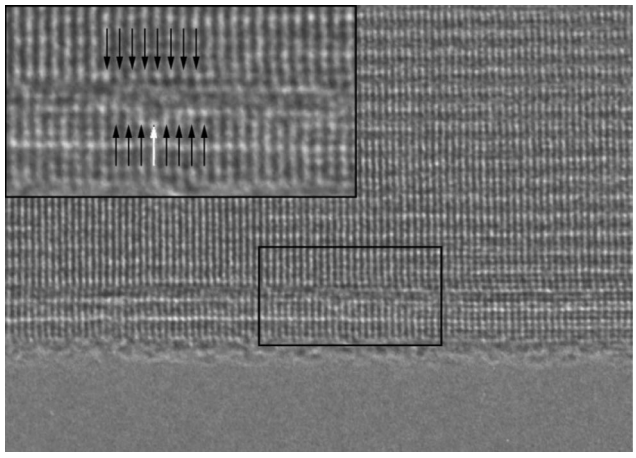

Figure 10. High-resolution TEM image PT6[101] zone axis of a crystal rod of IZM-1. At the edge of the crystal a lattice shift by 1/2 *c* along the channel direction is observed. The offset occurs over several layers with absent fringes indicating an elastic relaxation of the lattice rather than a sharp fault plane of PT1 in PT6.

Table 2. Lattice Energies and Compliance to Shear of PT1, PT3, and PT6

		compliance to shear (1/MPa)			
		∥ channel			
	lattice energy with respect to α-quartz (kJ/(mole T atom))	*xz* plane	*yz* plane	layer plane	⊥ channel
PT1	9.04	30.3	32.3	31.5	31.3
PT3	8.43	34.0	29.5	29.6	29.6
PT6	7.62	32.6	30.1	30.0	70.7

been caused by shear forces during growth, which resulted in failure to connect neighboring tubes at the position indicated by a white arrow in Figure 10. Most surprisingly, in isolated crystal rods, almost no evidence for PT1 was found despite its presence in the sample as indicated by PXRD, and specifically by the ED pattern of aggregated rods. In this sample, the degree of aggregation of individual crystallites is much more pronounced as in the COK-8, consisting of nanoneedles. Correspondingly, the detected average content of PT1 is increased as also indicated by analysis of the X-ray diffraction patterns.

Rationalization of Observations by Simulation. In all studied samples, PT6 is present in significant amounts, whereas the presence of other PTs (PT1 in samples 1 and 2 and possibly PT3 in the seeds) and planar faulting are observed in either aggregates of PT6 crystallites or at the rims of large crystals. To understand this observation, lattice properties of the purely siliceous topologies were calculated using the GULP program.[32−35] The obtained lattice energies of the PTs relative to α-quartz are listed in Table 2. These values are in good agreement with the well-established relationship between framework density and lattice energy and can, therefore, be treated as reliable qualitative means of comparison of the different topologies.[36,37,42,44] As all polytypes have identical (5,0) silica tube pore geometry, any difference in energy can only be due to the different connections between these channels and the resulting differences in T-dimer arrangement. Depending on the relative position of tubes along the channel direction neighboring pores either connect via 4-rings (4R) or via zigzag crankshaft chains (CS). Among all polytypes, PT1 and PT6 take special roles: their pores are exclusively connected by either CS (PT1) or 4R (PT6) configuration in a simple tiling of the rhombs made up from 4 tubes (Figures 1 and 2).

Of all polytypes PT6 has the lowest lattice energy, whereas PT1 has the highest. Compared to PT1 the calculated energy of PT6 is about 1.4 kJ/(mol Si atoms) lower. This result indicates the connectivity between pores by 4R is energetically more favorable than the CS arrangement. PT6 therefore will be obtained if the synthesis occurs close to isotropic thermal equilibrium conditions. Such conditions are obviously approached during PT6 crystallite formation and growth in COK-8 and IZM-1.

The occurrence of PT1 in these samples, therefore, must be caused by local deviations from equilibrium. Likely suspects are directional shear forces in needle aggregates caused by slight misalignments between individual needles. An inspection of the compliance matrix of PT6 reveals a peculiarity only observed for this structure. This lattice readily yields to shear-forces perpendicular to the channels causing a deformation of the angle β between the *a* and *c* axis. The lattice can respond by elastic deformation of *a*, *c*, and β to shear along *a* and/or *c* in the *ac* plane. The same distortion applied along needle axis, the *b* direction, causes more than twice the shear stress, which can eventually lead to structural failure of the PT6 lattice. Because of the relation between the different PTs translation by 1/2 *b* of a row of channels of PT6 in the *ab* and *bc* plane directly results in the formation of PT1 and vice versa using the respective lattice directions (Figure 2, Table 2).[44] This might explain why these two PTs are observed in the aggregates of needles and rods in COK-8 and IZM-1 samples, whereas isolated crystallites are composed of pure PT6. The use of seeds facilitated the growth of very thin PT6 needles in the COK-8 sample and limited the faulting typically observed in thicker needles.

In this context it should be mentioned that a shearing along the channel direction in the plane of connected layers ((111) plane of PT6) would lead to PT3 instead of PT1 (Table 2). The lattice stiffness towards shear in this plane in channel direction is very comparable to the values in *ab* and *bc* planes. The proven absence of PT3 in samples COK-8 and IZM-1, therefore, most likely is a result of the needle and rod shape. From the high-resolution images (Figures 8 and 10), it can be derived that most of the crystallites terminate in and connect via {101} planes, corresponding to sheets of directly linked pores.[44] Also, it was observed that local faulting occurs preferentially at the edges of the crystals. If during aggregation of the individual needles and rods stress in needle axis occurs and structural failure is imminent, the crystallites will break where they are thinnest, at their corners. In crystals terminated by {101} faces, break and shift will first occur at the edges in the *ab* or *bc* planes, resulting in the local formation of PT1 (Figure 11, left).[44]

(42) Piccione, P. M.; Yang, S.; Navrotsky, A.; Davis, M. E. *J. Phys. Chem. B* **2002**, *106*, 3629.
(43) Navrotsky, A. *Curr. Opin. Colloid Interface Sci.* **2005**, *10*, 195.
(44) A visualization of the shearing mechanism can be found on http://www.biw.kuleuven.be/cok/polytypes.html.

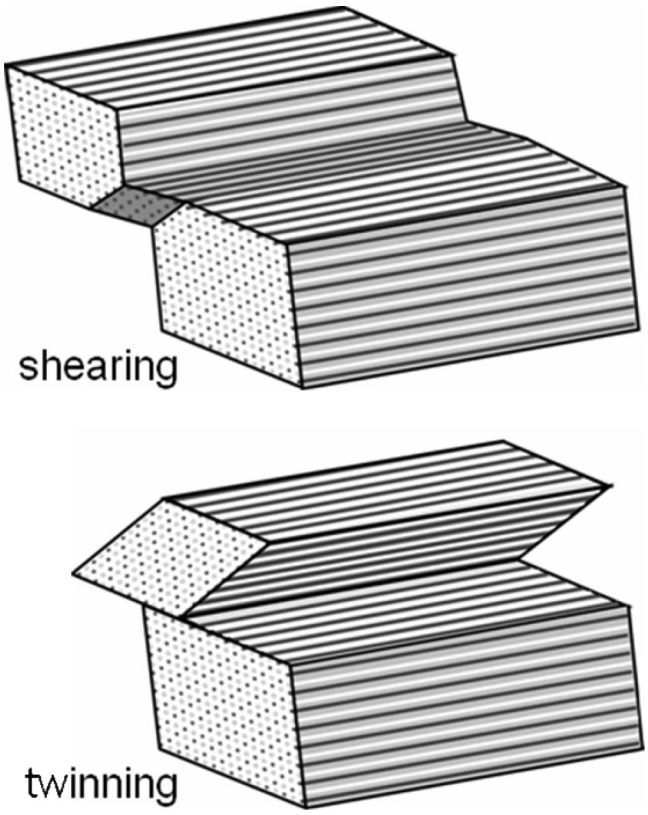

Figure 11. Illustration of possible faulting mechanisms during sideways aggregation of PT6 needles terminated by {101} faces.

Another lattice fault to be expected from stacking PT6 crystals via their 101 faces would be twinning (Figure 11), which can best be observed in channel direction, unfortunately inaccessible in the here studied needlelike morphologies. However, extensive twinning has been observed by Kirkland et al. in ZSM-48 samples with different morphology.[12]

Lobo and van Koningsveld tried to simulate this selected area electron diffraction pattern along the pore direction (Figure 12b).[23] By using the DIFFax[40] program in which the disorder was tuned by three distinct fault probabilities, a diffraction pattern was reproduced as shown in Figure 12b. But as the corresponding high-resolution image clearly shows extensive PT6{101} twinning, this diffraction pattern could be simply regarded as an overlap of two diffractions patterns from a defect free area, one being transformed by a mirror plane (twinning plane) with respect to the other, as shown in Figure 12c. Because of the geometry ratio, the diffraction spots of the 3n rows fall at almost exactly the same positions for the two diffraction patterns. Comparing with the model of statistic faulting and intergrowth of several polytypes, the twinning model shows a better agreement of simulated spot positions with the experimental diffraction pattern obtained by Kirkland et al.[12]

It was also reported that other zeolite materials are formed through the aggregation of nanosized crystallites.[41] In the case of ZSM-22 zeolite, at first nanoneedles are formed and grow along their long axis until the framework sources are exhausted.[41] The corresponding enrichment of aluminum in the outer regions of these nanoneedles results in a very specific distribution of catalytically active sites during the later occurring side-wise aggregation of these needlelike building units. In the current work, it became obvious that not only the chemical but also mechanical conditions can have a direct influence on the properties and structure of the finally obtained material.

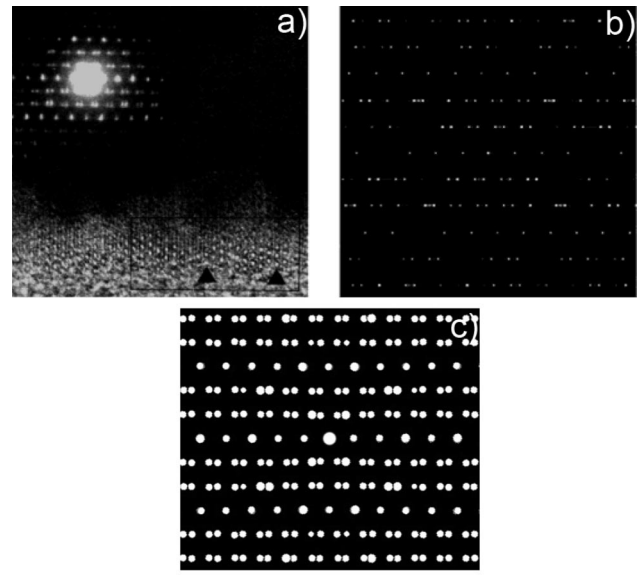

Figure 12. (a) Selected area electron diffraction pattern along channel direction published by Kirkland et al.,[12] (b) its interpretation as intergrowth by Lobo et al.,[23] and (c) its interpretation as extensive PT6{101} twinning.

Conclusions

Simulation of high-resolution TEM enabled the identification of PT1 and PT6 in disordered materials belonging to the ZSM-48 and related zeolites family. The use of large amounts of seeds in a synthesis procedure for ZBM-30 led to the crystallization of COK-8, representing the PT6 endmember of the polytypical zeolite family. IZM-1 synthesized in ethyleneglycol medium presents PT6 as major phase in a block like arrangement with PT1. Lattice energy estimations indicate that PT6 is the most stable polytype. The use of seeds consisting of an intergrowth of PT6-PT3 or substantially disordered PT6 results in the growth of phase pure PT6. The observed phase purity is linked with crystal morphology. Thin needles tend to be phase pure. Thicker crystals seem to form by alignment and fusion of nanoneedles being prone to formation of stacking errors leading to local PT1 ordering. Mechanical aspects need to be considered when stacking zeolite building blocks into materials.

Acknowledgment. C.E.A.K., J.A.M., and G.V.T. acknowledge FWO Vlaanderen for project funding and the Flemish government for supporting a concerted research action (GOA). C.E.A.K. and J.A.M. acknowledge funding by the Belgian Prodex office.

Supporting Information Available: High-resolution image simulation of PT6 and PT1 along different orientations (PDF). This material is available free of charge via the Internet at http://pubs.acs.org.

CM802614X